ChemPubSoc Europe

DOI: 10.1002/open.201600102

Open Access ChemistryOPEN Full Papers

Insights into Biochemical Alteration in Cancer-Associated Fibroblasts by using Novel Correlative Spectroscopy

Saroj Kumar,*[a, b, c] Xia Liu,[c] Ferenc Borondics,[d] Qunfeng Xiao,[c] Renfei Feng,[c] Erik Goormaghtigh,[e] and Fredrik Nikolajeff[a]

The microenvironment of a tumor changes chemically and morphologically during cancer progression. Cancer-stimulated fibroblasts promote tumor growth, however, the mechanism of the transition to a cancer-stimulated fibroblast remains elusive. Here, the multi-modal spectroscopic methods Fourier transform infrared imaging (FTIRI), X-ray absorption spectroscopy (XAS) and X-ray fluorescence imaging (XFI) are used to characterize molecular and atomic alterations that occur in cancer-stimulated fibroblasts. In addition to chemical changes in lipids (olefinic and acyl chain) and protein aggregation observed with FTIRI, a new infrared biomarker for oxidative stress in stimulated fibroblasts is reported. Oxidative stress is observed to cause lipid peroxidation, which leads to the appearance of a new band at 1721 cm^{-1}, assigned to 4-hydroxynonenal. Complementary to FTIRI, XFI is well suited to determining atom concentrations and XAS can reveal the speciation of individual elements. XFI reveals increased concentrations of P, S, K, Ca within stimulated fibroblasts. Furthermore, XAS studies reveal alterations in the speciation of S and Ca in stimulated fibroblasts, which might provide insight into the mechanisms of cancer progression. Using XFI, not only is the concentration change of individual elements observed, but also the subcellular localization. This study demonstrates the wealth of biochemical information provided by a multi-modal imaging approach and highlights new avenues for future research into the microenvironment of breast tumors.

1. Introduction

Breast cancer is a major global health issue. It has the highest rate of incidence in Western women and is the second major cause of their mortality. It causes extensive individual suffering and is a huge burden on health care in society.[1] The major cause of death in breast cancer is due to malignancy, where confined cancer cells inside the mammary ducts, spread outside into the stroma. These cancer cells later come in contact with blood vessels or the lymphatic system and become metastases that are unfortunately usually incurable. A recent study showed that an early diagnosis together with the relevant therapy reduce metastasis and patient mortality.[1] To prevent metastasis, it is therefore necessary to diagnose at an early stage and begin adjuvant therapy. Currently, several modes of therapy are in practice, including radiotherapy, chemotherapy and antibody therapy. These therapies primarily target the cancer cells and preserve the healthy cells from the surrounding environment of the stroma.[2] The stroma consists of the cellular tissue network and the extracellular matrix (the collection of molecules secreted by the cells). Cancer cells induce significant changes into the normal stroma in order to turn into reactive stroma.[3] In early tumor development, cancer cells are confined to the mammary duct by the basement membrane and stroma, which is connected through the pores and the gated channel becomes respondent to cancer progression.[1,4] The mechanism by which cancer cells transform the normal stroma into the reactive stroma is not fully understood. Among several stromal components, fibroblasts are considered to have a significant role in cancer progression.[5] Cancer-stimulated fibroblasts (SFs), better known as cancer-associated fibroblasts (CAFs), are present in stroma near to the ductal carcinoma in situ, the condition prior to metastasis, and differ from those in normal breast tissue.[3,6] Previous studies[6–9] have shown the role of SFs in cancer progression by enhancing secretion of growth factors such as hepatocyte growth factor, transforming growth factor and insulin-like growth factor as well as metalloproteinases. Thus, understanding the interac-

[a] Dr. S. Kumar, F. Nikolajeff
Berzelii Technology Centre for Neurodiagnostics
Department of Engineering Science
Uppsala University, Uppsala 75105 (Sweden)
E-mail: sarojgupta.k@gmail.com

[b] Dr. S. Kumar
Department of Biophysics, All India Institute of Medical Sciences
New Delhi 110029 (India)

[c] Dr. S. Kumar, X. Liu, Q. Xiao, R. Feng
Canadian Light Source
Saskatoon, SK S7N 2V3 (Canada)

[d] F. Borondics
SOLEIL Synchrotron
91190 Gif-sur-Yvette, Ile-de-France (France)

[e] E. Goormaghtigh
Structure and Function of Biological Membranes (SFMB)
Université Libre de Bruxelles (Belgium)

tions of cancer cells with the microenvironment might significantly improve progression towards new cancer treatments.

Several metal ions play major roles in the balance of cellular environments, and alterations to these ions affect cell proliferation and differentiation, including cancer progression.[9] Furthermore, the roles of K and Ca ion channels as well as the roles of intracellular Ca in cancer cell lines and breast cancer progression have been reported.[10] It is also known that sulfur in its different forms has a role in cancer progression.[11,12] Among the presently available methods, gene-based characterization of cancer cells is most promising; however, it is expensive and is of limited use for characterization at the single-cell level due to tumor heterogeneity.[13] Therefore, it is essential to work towards effective and economical alternative methods to characterize the role of the microenvironment in cancer progression at the cellular level and especially that of the fibroblast.[7,14]

The combination of infrared microspectroscopy,[7,15,16] synchrotron X-ray absorption spectroscopy (XAS)[17,18] and X-ray fluorescence imaging (XFI)[18] can help to analyze cells in situ and localize the biochemical changes at cellular and subcellular spatial resolution. Previous studies on fibroblasts[7,15,16] have shown infrared spectral modifications in fibroblasts in the presence of breast cancer cells. In this study, for the first time, we identify an infrared biomarker for oxidative stress in SFs. By combining XAS and XFI into these studies, our research methods not only reveal element concentrations, but also highlight alterations in the chemical forms of different elements, which increases the ability to connect chemical alterations with possible mechanistic roles in cancer progression.

Experimental Section

Cell Lines and Growth Conditions

Cells of the fibroblast cell line CCD-1126Sk, established from normal human breast tissue were obtained from the American Type Culture Collection (ATCC). MCF-7 breast cancer cells were also obtained from the ATCC. Iscove's modified Dulbecco's medium (IMDM), fetal calf serum (FCS), trypsin–EDTA buffer, and penicillin–streptomycin were purchased from Lonza (Toronto, Canada). Cells were grown in the conditioned media, which contained IMDM supplemented with 1% penicillin–streptomycin and 10% FCS in a humidified incubator supplied with 5% CO_2 at 37 °C.[19] Cells were grown initially in T25 flasks and later transferred into the T75 flasks. The medium was changed twice or three times per week. Once the cells reached a sub-confluence level (cell count around 60–75% of the total area of culture plate), they were transferred into fresh culture flasks. Cells were detached by using trypsin–EDTA (trypsin: 0.5 g L^{-1}; EDTA: 0.2 g L^{-1}) buffer for 3–5 min after incubation at 37 °C.

We co-cultured the fibroblasts with breast cancer cells with no contact between the two cell lines. We grew the fibroblasts on a CaF_2 window (transparent to infrared radiation for the FTIR measurements) and the cancer cells on a LEXAN film (transparent to X-rays for XAS and XFI measurements), which lay on the bottom of a 12-well plate culture box. LEXAN film is a metal-free polycarbonate membrane sheet approximately 100 μm thick that has no negative influence on cell growth. Fibroblasts and cancer cells were first grown for 5–6 h in different wells of the culture box to allow the cells to settle on the surface, and then the CaF_2 window and LEXAN film with the fibroblasts attached to the upper surface were transferred into the wells in which cancer cells were growing. During this process, the two types of cells were in contact only through the medium. Prior to FTIR and X-ray measurements, the disks with the fibroblasts were washed with distilled water and dried (2–3 min) with the help of a gentle flow of N_2 gas and the measurements were completed within 3–4 h. It has been shown previously that drying the fibroblast cells largely preserves spectral differences;[19] here drying was followed in a similar manner on CaF_2 and LEXAN surface. For XAS measurements, we centrifuged both the normal fibroblasts (NFs) and SFs and then transferred the pellets onto LEXAN film surface, which was dried before the measurement.

FTIR Imaging Measurements

Infrared data were acquired in the transmission mode by using a Hyperion 3000 FTIR imaging system (Bruker Optics, Ettlingen, Germany). This system is equipped with a 64×64 focal plane array detector, which is a liquid-nitrogen-cooled mercury–cadmium–telluride detector, with an upper objective of 15× magnification and a numerical aperture of 0.4, and a lower condenser of 15× magnification and 0.4 numerical aperture. The spectral resolution was set to 4 cm^{-1}. One unit image covers an area of 170×170 μm^2 in the sample regions, resulting in 4096 spectra; each being the average of 500 scans recorded in approximately 8–10 min. All the experimental data were acquired by using OPUS software (Bruker) at room temperature. Each sample spectrum was ratioed against a background spectrum obtained in the absence of sample. Mapping larger areas was achieved through mosaicking (typically 2×2 or 2×3 unit images).

FTIR Data Analysis

All spectral processing and classifications were carried out using the program Kinetics written by our group and running under Matlab (Mathworks Inc, Natick, MA). All the spectra were pre-processed as described previously.[20] The water vapor contribution was subtracted as described previously[21] with 1956–1935 cm^{-1} as a reference peak. Spectra were normalized to equal area between 1725 and 1481 cm^{-1}. An 11-point baseline passing by 3620, 2995, 2800, 2395, 2247, 1765, 1724, 1480, 1355, and 1200 cm^{-1}, was subtracted.[22] Raw spectra were vector-normalized to the amide I band (1700–1610 cm^{-1}), and second derivatives were calculated with a Savitsky–Golay nine-point smoothing average.

Synchrotron XAS Data Collection

P, S, K, and Ca K-edge spectra of SFs and NFs were collected to observe the effect of exposing fibroblasts to cancer cells. The spectra were collected at the Canadian light source, using the soft X-ray microcharacterization beamline (SXRMB, http://sxrmb.lightsource.ca/) and using a Si(111) double-crystal monochromator. The incident beam was reduced to an area of 2×4 mm^2 using vertical and horizontal slits, and intensity was measured with a He-filled I_0 ion chamber. Samples were mounted at 45° to the incident beam, and X-ray fluorescence collected with a four-element Si drift diode detector. Prior to spectra collection, the sample chamber was purged with He gas. All spectra were recorded at ambient room temperature. Al K-edge spectra, P (2140–2180 eV), K (3600–3640 eV), Ca

(4018–4068 eV) and S (2452–2502 eV), were recorded with 0.2 eV energy steps and an integration time of 4 s per energy point.

Synchrotron XAS Data Analysis and Processing

P, S, K, and Ca K-edge spectra collected from SFs and NFs were normalized to the edge jump to observe the overall elemental differences. For the Ca speciation, we used the XAS spectra of reference compounds (calcium pyrophosphate, calcium carbonate, hydroxyapatite, calcium hydroxide and calcium oxide) to facilitate identification of the different forms present in the both samples (SF, NF) by linear combination fitting. Fitting was performed with Athena software, a free online software available for X-ray data manipulation.[23] Prior to fitting, the spectra were baseline subtracted and normalized.[23] To determine the sulfur metabolome in SFs and NFs, the XAS spectra were fitted to a linear combination of model compounds containing disulfides (oxidized glutathione), thiols (reduced glutathione), thio-ethers (methionine), sulfoxides (methionine sulfoxide), sulfinic acids (hypotaurine), sulfonic acids (taurine), sulfate ester (dextran sulfate) and inorganic sulfate (sodium sulfate). Spectra were fitted using DATFIT from the EXAFSPAK program package.[24] The sulfur-containing model compounds used in this study were selected from previously published data.[17]

Synchrotron XFI Data Collection and Processing

Elemental maps of the SF and NF samples were collected using XFI at the VESPERS beamline (http://www.lightsource.ca/beamlines/vespers.php), Canadian Light Source. A polychromatic beam covering 6–30 keV with a beam size of 3 μm was used for the measurements. Samples were positioned 45° to the incident beam, and the emitted X-ray fluorescence was recorded by a four-element Vortex silicon drift detector, which was placed approximately 40 mm from the sample at 90° to the incident beam. Raster scans were performed by a set of motorized stages in step-by-step mode with a step size of 4 μm and an integration time of 5 s per pixel. The flux of the incident beam was monitored by using a N_2-filled ionization chamber for normalization. The four channels of XRF spectra at each sample position were recorded and dead-time-corrected individually, then summed. The normalized peak areas of each characteristic emission lines in these spectra were used to generate maps of the elements of interest. The data were processed by using Sam's Microanalysis Toolkit (http://smak.sams-xrays.com/).

Statistical Analysis

A paired *t*-test was performed to obtain significant differences between the molecular content of the different samples. As multiple *t*-test comparisons were used, the *p* value obtained was multiplied by the number of *t*-tests performed to control for family-wise error. All *t*-tests were two tailed and the 95% confidence limit was used to test for significance.

2. Results and Discussion

2.1. IR Imaging of Fibroblasts Stimulated with Cancer Cells without Direct Contact between the Cells

Human breast fibroblasts were grown for different time periods (24 and 72 h) on a CaF_2 window in the presence (stimulated) or absence (normal, control) of cancer cells, but with no direct contact between the cell types as explained in the Experimental Section.[7] A representative bright-field image of a fibroblast and the corresponding FTIR image of protein content (by using the intensity at 1654 cm^{-1}) are presented in Figure 1A. A comparison of representative second-derivative spectra from a normal fibroblast and fibroblasts stimulated by cancer cells for 24 and 72 h, is shown in Figure 1B (1750–1400 cm^{-1}) and Figure 1C (3050–2800 cm^{-1}). A comparison of these spectra reveals numerous spectroscopic differences. Most notably, an increased area under the curve was measured for second-derivative bands centered at 1721 and 1632 cm^{-1} with increased time; these have been assigned to ν(C=O) of aldehydes and the amide I band of protein aggregates,[25] respectively (vide infra). A decreased area under the curve was also measured for the average spectrum of fibroblasts stimulated with cancer cells for 72 h assigned to lipids, that is, bands centered at 3010 [olefinic ν(C=CH)], 2922 [methylene ν_{as}(C–H)], and 1735 cm^{-1} [ester ν(C=O)]. In addition to the differences between the normal and stimulated fibroblasts with increased time, there appeared to be a correlation between the time of stimulation and magnitude of the difference, with the greatest differences observed in cells stimulated for 72 h compared to 24 h. FTIR analysis was performed for five-cell replicates for each treatment group, and the spectroscopic differences described above were observed to be statistically significant (Figure 1D and E). These differences suggest that oxidative stress is a component of cancer cell stimulation of fibroblasts, resulting in oxidative damage to lipids and decreased lipid content, and the accumulation of lipid oxidation products (aldehydes) and protein oxidation products (aggregated protein).

2.2. A New IR Biomarker of Oxidative Stress is Observed in Fibroblasts Stimulated with Cancer Cells

This study revealed the presence of a distinct peak at 1721 cm^{-1} in cancer-stimulated fibroblasts, which was not present in normal fibroblasts. Furthermore, this peak increased in intensity if the fibroblasts were exposed for longer periods to cancer cells (i.e., 72 vs. 24 h). Quantification of the carbonyl ester (1735 cm^{-1}) and aldehyde (1721 cm^{-1}) bands confirmed that these changes were statistically significant, lipid ester groups, reducing from $3 \pm 0.18 \times 10^{-2}$ to $2 \pm 0.15 \times 10^{-2}$; and aldehyde increased from $1 \pm 0.05 \times 10^{-3}$ to $11 \pm 0.65 \times 10^{-3}$, in SFs relative to the NFs. Additionally, a concomitant decrease in the ester carbonyl peak intensity (1735 cm^{-1}),[26] was observed (Figure 1D and Table 1), suggesting a possible chemical relationship. We propose that the appearance of the peak at 1721 cm^{-1} in SFs might arise from aldehyde carbonyl stretching of 4-hydroxynonenal (4-HNE), a biomarker of lipid peroxidation.[27] The FTIR spectrum of 4-HNE has been shown to also display a characteristic peak at 1440 cm^{-1} (Figure 1B), assigned to C–H bending in CH_3 groups of 4-HNE. As shown in Table 1, an increased area under the curve in the second-derivative spectrum was also observed at 1440 cm^{-1} in SFs, providing additional support for 4-HNE production during fibroblast stimulation.

We speculate that the amount of 4-HNE is increased due to oxidative stress derived from overproduction of reactive

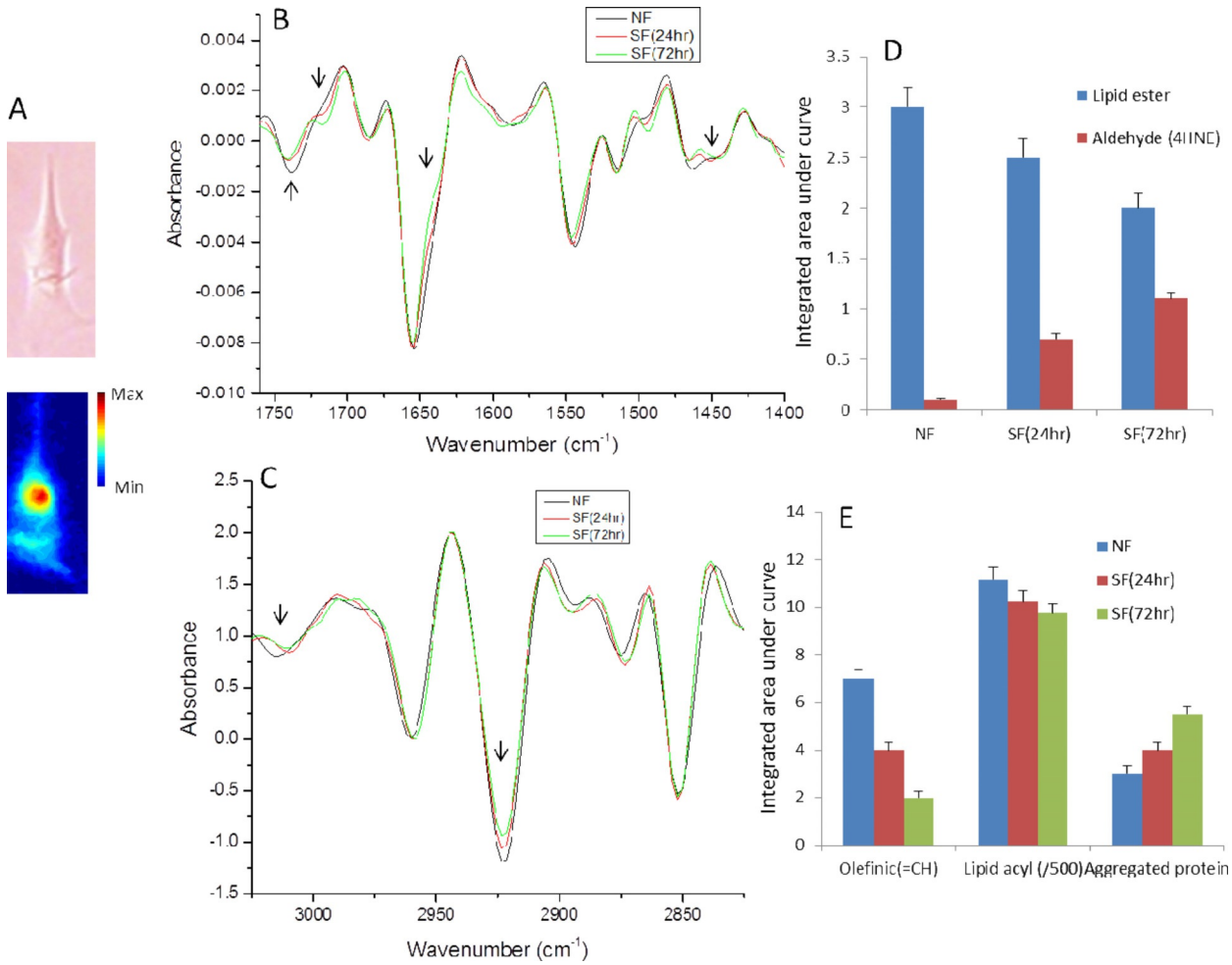

Figure 1. FTIR imaging of biochemical changes in cancer-stimulated (SF) and normal (NF) fibroblasts. A) Upper panel: Brightfield microscopy image of a single fibroblast; lower panel: a typical IR image of a fibroblast generated by using the infrared absorbance at 1654 cm^{-1}. B and C) Representative of the average second-derivative (1750–1400 cm^{-1}) spectra from the NFs (blue) and SF after 24 h (red) and 72 h (green) simulation. Arrows in panel B (left to right) indicate bands at 1735 and 1721 cm^{-1} from ν(C=O) of lipid ester and aldehyde, band in the amide I region at 1632 cm^{-1} from the aggregated protein (β-sheets) and at 1440 cm^{-1} from the ν(C–H) of CH_3 groups, respectively. Similarly, arrows in panel C indicate bands at 3010 cm^{-1} from olefinic ν(=CH) and at 2922 cm^{-1} from ν_{as}(C–H) of the CH_2 groups in the lipid acyl chain, respectively. D and E) Statistical analysis of the integrated area under the curve (IUPAC) for lipid (ester, acyl chain and olefinic), aldehyde and aggregated protein absorption bands. E) The value of lipid acyl chains in divided by a factor of 500 to simplify visual comparison. Statistical significance was determined from four replicates ($n=5$) with paired *t*-test and 95% confidence.

Table 1. Second-derivative FTIR spectral intensity analysis of relative levels of lipid peroxidation. Normal fibroblasts (NFs) and stimulated fibroblasts (SFs) exposed to breast cancer cells (MCF-7) over different time periods. Data is shown as mean ± SD ($n=5$). Significant differences were tested using a two-tailed unpaired Student *t*-test with a 95% confidence limit ($\rho<0.05$).

Cell line	Lipid ester (C=O vibration, 1755–1725 cm^{-1})	4-Hydroxynonenal (1725–1705 cm^{-1})
NF	$(3\pm0.18)\times10^{-2}$	$(1\pm0.05)\times10^{-3}$
SF (24 h)	$(2.5\pm0.15)\times10^{-2}$	$(7\pm0.35)\times10^{-3}$
SF (72 h)	$(2\pm0.15)\times10^{-2}$	$(11\pm0.65)\times10^{-3}$

oxygen species (ROS), such as singlet oxygen ($^1O_2$), superoxide radical ($^{\bullet}O_2^-$), hydrogen peroxide (H_2O_2), and hydroxyl radical ($OH^{\bullet}$). Singlet oxygen can cause oxidation of proteins, polyunsaturated fatty acids, and DNA. Hydroxyl radicals can react with many biomolecules such as lipids, proteins, and nucleic acids, in almost all cellular organelles.[28] These current data suggest that future studies can use FTIR spectroscopy to direct relative changes in 4HNE production, during chronic oxidative stress, to test the hypothesis that chronic oxidative stress might contribute to a higher incidence of breast cancer metastasis.[27] Previous studies have reported alterations in intensity of the band centered at 1440 cm^{-1}, where it was observed that higher absorbance of this band correlated with a more severe tumor grade.[29] It was postulated in the previous study that these changes might be related to changes in the extracellular matrix.[29]

2.3. General Features of Synchrotron Micro-XANES Spectra of Different Elements in Normal Fibroblasts and Fibroblasts Stimulated with Cancer Cells

To provide insights into the chemical nature of different elements such as P, K, Ca, and S, XANES measurements were performed at the K-edges of these elements for the NF and SF samples (Figure 2). Exposure of the SF sample for 72 h to the MCF-7 cancer cells was compared against the NF sample. The spectra of NFs and SFs for each element were normalized to observe the overall differences in the concentration. We observed minimal differences in P concentrations, which were 20% higher in SFs. To emphasise the differences in concentrations of the elements K, Ca and S, we ratioed the concentrations of these elements against the P concentration, to minimize the errors that might arise due to the sample thickness. The overall concentration of K and S (Figure 2B and D) was increased by approximately 1.8 times, whereas the Ca concentration (Figure 2 panel C) increased by approximately 2.3 times in SFs (cancer stimulated) compared to the NFs (control sample). The findings of increased concentration of these elements in SF are an indication of the different cell activity in SFs compared to NFs. Increased concentrations of Ca and K might be related to higher cell differentiation and proliferation. Ion channels play a critical role in cell migration.[30] In particular, voltage-gated K^+- and Ca^{2+}-activated channels are associated with cell adhesion and migration in cancer, including breast cancer, melanoma leukemia, and others.[9,10,30] Activation of K^+ channels hyperpolarizes the membrane potential, which increases Ca^{2+} influx, and the link to cancer progression has been reported.[31] Ca regulates cell migration and it is known that highly metastatic breast cancer cell lines (MB-231) are calcium dependent.[32] Previous studies have found that several types of K^+ channels, activated by intracellular Ca^{2+} and ATP, are expressed in human breast cancer cells (MCF-7).[33–35] During tumorigenesis the breast tissues show K^+ channel overexpression by many fold (three to 100-fold).[34] A previous analysis of breast cancer patient blood and urine showed elevation of phosphate levels.[36] Several bioactive lipids such as sphingosine 1-phosphate and lysophosphatidic acid, which has growth-factor-like activity, are crucial in inflammation, and have roles in breast cancer development; also these lipids are naturally produced in fibroblasts.[37,38] C-reactive protein (CRP) upregulation by sphingosine 1-phosphate has a role in cell invasion.[38] Similarly, the increased concentration of S in SFs has been shown to affect cell proliferation and invasion. Proteoglycans (PG) are a key component of the extracellular matrix and have a crucial role in tumor progression and metastasis. Chondroitin sulfate PGs are directly associated with cellular function by modulating growth factors and cytokines.[39–40] The presence of different form of Ca and S and their possible role in the cancer progression and invasion will be discussed later.

Thus, in the cancer-stimulated fibroblast, an almost twofold increase in Ca, K and S concentrations as well as elevated P,

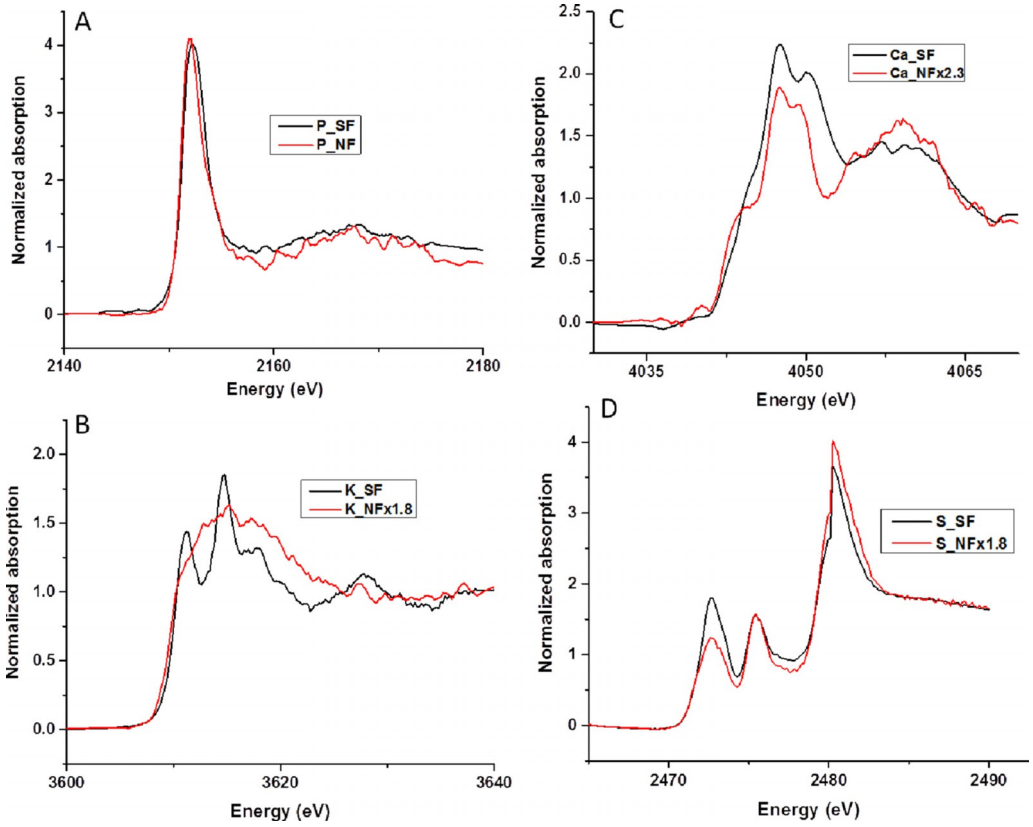

Figure 2. K-edge X-ray absorption spectra (XAS) to observe the elemental concentration changes in cancer-stimulated (SF) and normal (NF) fibroblasts. The spectra were normalized for visual representation. A) XAS spectra from element P, the concentration was 20% higher in SFs than in NFs. B–D) Spectra were ratioed by the elemental change in P to avoid the thickness error.

could be an indication of changes the cell activities and that might have a role in cell migration, proliferation and cell cycle activation which could enhance the breast cancer progression.

2.4. Synchrotron XAS Analysis of the Effect of Cancer Cells on Fibroblasts on the Calcium Speciation

To obtain insights into the chemical nature of calcium, and to determine the proportions of the different forms of calcium in the NFs (Figure 3A) and SFs (Figure 3B), bulk XAS spectra were collected at the Ca K-edge. These spectra were fitted to a linear combination (using the Athena software) of the pure spectra of the representative compounds calcium pyrophosphate ($Ca_2P_2O_7$), calcium carbonate ($CaCO_3$), hydroxyapatite (HA), calcium hydroxide [$Ca(OH)_2$], and calcium oxide (CaO; Figure 3C). Levels of calcium species are expressed (Table 2A) as the percentage of the total calcium detected in the SFs and NFs. In Figure 3D, a bar graph shows a clearer visual comparison of the amounts of these pure compounds in the SFs and NFs with the errors. We observed that the calcium pyrophosphate, HA and calcium hydroxide concentrations increased in the SFs compared to NFs. The calcium pyrophosphate, HA and calcium hydroxide account for 35.9, 23.7 and 10.9%, respectively, of total Ca in SFs, whereas for NFs (control) these Ca salts account for 12.4, 16.1 and 0%, respectively. We observed that the calcium carbonate concentration was decreased in SFs relative to that in NFs. We did not detect calcium oxide in either sample. The role of HA was found to enhance tumor cell migration.[41] Micro-calcification in breast cancer where calcifications are composed of calcium phosphate (pyrophosphate, HA) were previously reported[41]. We observed in SFs that the concentrations of calcium carbonate were decreased and HA increased. This findings are in line with a previous report that calcium carbonate amounts were lower in malignant ducts[42] and increased with the lesion grades.[43] It was established that HA influences the microenvironment by promoting mitogenesis and metalloproteinase expression in breast cancer.[44] The biological effects of HA on the surrounding cells has been reported, as well as on the upregulation of cytokines in the mammary cells, which leads to cancer progression.[44] The calcium hydroxide amount was higher in SFs than in NFs. The role of this form of calcium with cancer has not been properly reported, however genotoxic effects on human fibroblasts have been established.[45]

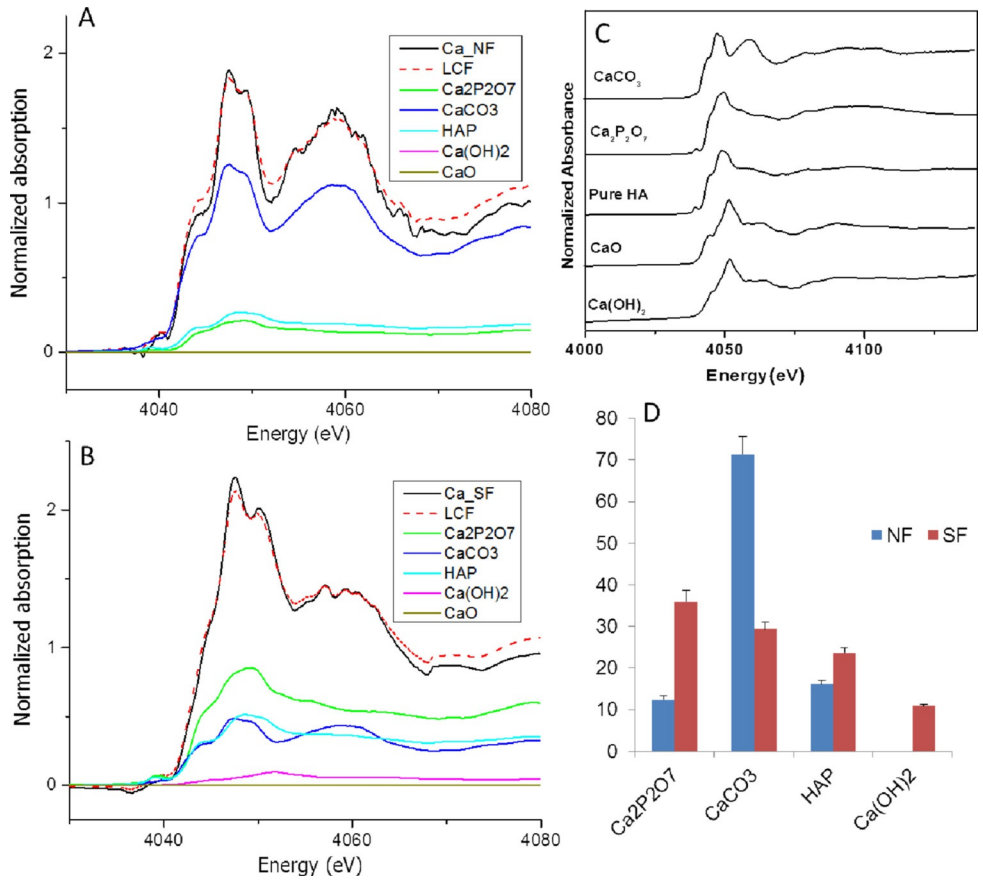

Figure 3. Representative analysis of calcium K-edge XAS spectra collected from A) normal and B) cancer-stimulated fibroblasts fitted to a linear combination of standard K-edge XAS spectra. The normalized squares fit shown as the red line. The reference spectra of pure components (Figure 3A) were scaled to their relative contribution to the fit. C) Calcium K-edge X-ray absorption spectra are representative of calcium species. All spectra were normalized to the height of the edge-jump after background removal. Spectra were vertically scaled as indicated for clarity. D) Statistical analysis of the representative of the percentage calcium composition in cancer-stimulated fibroblasts (SF) and normal fibroblast (NFs).

Table 2. The values given are the percentage calcium (A) and sulfur (B) composition in stimulated (SFs) and normal fibroblast (NFs). The values in parentheses are the average estimated standard deviation from the individual fits (given as the last digit of the percentage), which are obtained from the diagonal elements of the covariance matrices and assuming a constant variance across the range of individual spectra. N.D. = Not determined.

(A) Fibroblast	$Ca_2P_2O_7$	$CaCO_3$	Hydroxyapatite	$Ca(OH)_2$	CaO
SF (72 h)	35.9(8)	29.3(6)	23.7(5)	10.9(4)	N.D.
NF	12.4(8)	71.4(6)	16.1(5)	N.D.	N.D.

(B) Fibroblast	Thiol	Thioether	Disulfide	Sulfoxide	Sulfinic acid	Sulfonic acid	O-Linked sulfate ester	N-Linked sulfate ester	Inorganic sulfate
SF	27(9)	13(6)	10.9(4)	19(4)	0.2(2)	25(2)	4.2(5)	0.6(3)	N.D.
NF	19(9)	8.3(6)	12(4)	20(4)	N.D.	33(2)	2.8(5)	N.D.	4.8(4)

2.5. Synchrotron XAS Analysis of the effect of Cancer Cells on Fibroblasts on the Sulfur Speciation

It has been reported that the near-edge spectrum collected from samples comprised of different chemical forms can be fitted to a linear sum of the individual spectra from the each pure component.[17] To determine the proportions of sulfur-containing compounds in the SFs and NFs, XAS spectra were collected at the S K-edge. These spectra (Figure 4A and B) were fitted to a linear combination of the pure spectra of compounds representative of thiols, thioethers, disulfides, sulfoxides, sulfinic acids, sulfonic acids and sulfates, using model compounds of sulfur previosuly described (sulfate esters and inorganic sulfate).[17] The relative concentrations of sulfur species are expressed (Table 2B) as the percentage of the total sulfur detected in the SFs and NFs. The bar graph in Figure 4C represents the amounts of these pure individual compounds present in the SFs and NFs with the standard deviation. Thiols, including glutathione, cysteine, and cysteine–glycine, play important roles in cellular processes such as cell differentiation, proliferation and imbalance in homeostasis of those involved in progression of disease, including cancer.[11,12] We observed a relative significant increase in the amounts of thiols (19 to 27) and thio-ethers (8.3 to 13) in the SFs. Elevated levels of glutathione were observed in various tumors, which is also associated with higher levels of glutathione-dependent enzymes.[12] A decreased thiol/disulfide ratio is characteristic of oxidative

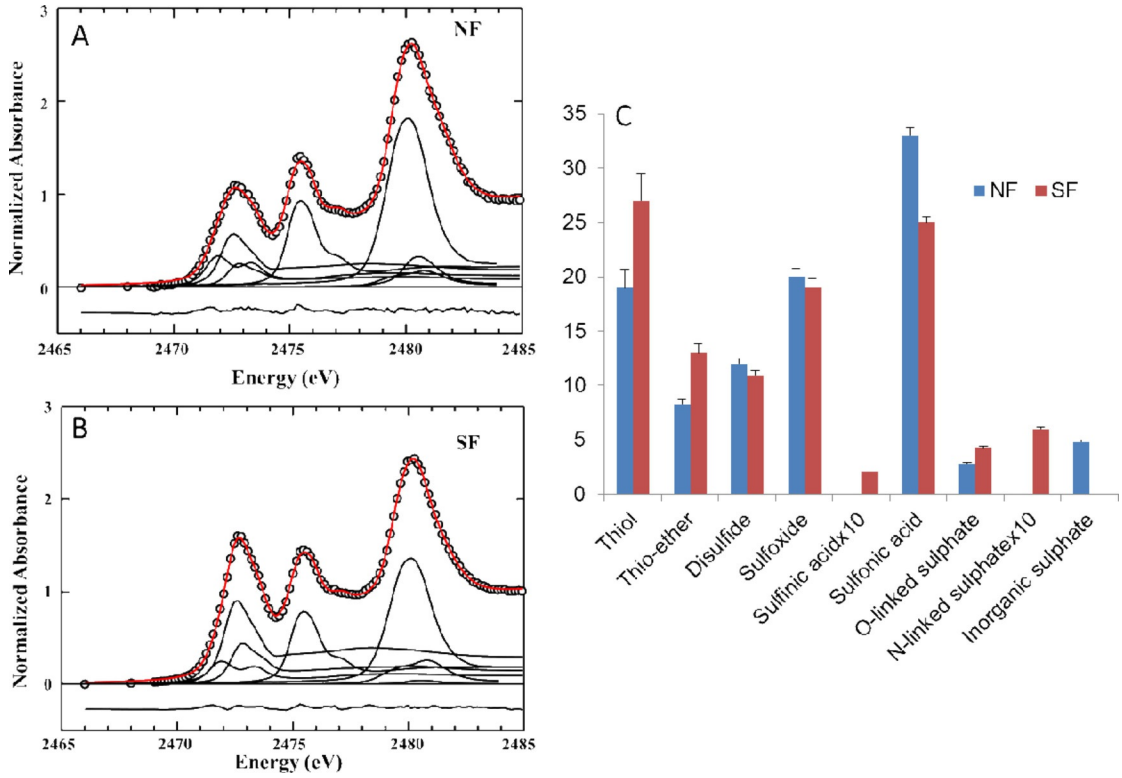

Figure 4. Representative analysis of sulfur K-edge XAS spectrum collected from A) normal and B) cancer-stimulated fibroblasts normalized to a linear combination of standard K-edge XAS spectra. The normalized squares fit is shown as the red line. The reference spectra of pure components (Figure 3B) were scaled to their relative contribution to the fit. C) Statistical analysis of the percentage calcium composition in cancer-stimulated fibroblasts (SF) and normal fibroblasts (NF).

stress[17,35] and has implications in tumor progression.[11] In oxidative stress conditions, free-radical oxygen species generation increases the cell injury, but a physiological level to maintain intracellular signaling pathways is essential for cell survival.[12] Thiols, including glutathione, which is considered as a physiological scavenger, and their relative increased levels in SFs are indicative of the protective mechanism against oxidative stress.[46] We exposed normal fibroblasts to cancer cells (MCF-7) for 72 h, which induced increased thiol levels in SFs, and could not observe the decreased thiol/disulfide ratio,[17] which indicates oxidative stress. Proteoglycan, which is located on the cell surface and extracellular matrix, comprises core proteins and a number of glycosaminoglycans. The modifications of O-linked and N-linked glycans depends on the changes in glycosyltransferase levels.[47] We observed the relative increased in amounts of the O-linked sulfate (2.8 to 4.2) in SFs compared with NFs. The overproduction of mucin glycoprotein in tumors has been reported, which is characterized by dense clusters of O-linked glycans.[47]

2.6. Synchrotron XFI Analysis of the Effect on Normal and Cancer-Cell-Stimulated Fibroblasts

SFs and NFs were analyzed by XFI at 4×4 μm spatial resolution. This method provided elemental differences (S, Ca and K) in the SFs relative to the NFs (Figure 5). We screened single fibroblasts from the both samples and it was observed that S, Ca and K concentrations tended to be higher in SF. For both samples, we scaled similarly to visually reflect the concentration changes. During the XAS analysis, we observed a relative increase in the concentration of these elements in both samples, which is also reflected here in the single fibroblast images. Figure 5 also shows the distribution of these elements throughout the fibroblasts. We observed that the localization of these elements are highest in the nucleus followed by the cytoplasm.

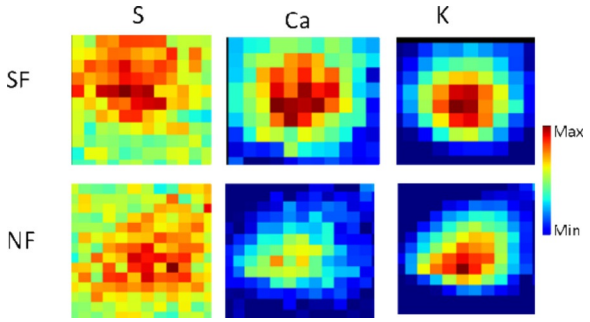

Figure 5. X-ray fluorescence imaging (XFI) elemental mapping of cancer-stimulated (SF, upper panel) and normal (NF, lower panel) fibroblasts. Elemental maps of S, Ca and K of a single fibroblast from both the samples. The color bar shows the concentration and localization of these elements. Each pixel is 4×4 microns in size.

3. Conclusions

This work entailed the use of multimodal imaging and spectroscopy techniques to investigate chemical changes as well as map the individual elemental concentrations in fibroblasts. The use of infrared microspectroscopy allows the chemical changes to be observed. Here, we demonstrate that oxidative stress leads to lipid peroxidation and observed a new infrared biomarker. Quantification of lipid degradation might be possible, which could also help to understand the nature of oxidative stress. The increased level of protein aggregation was less clear and that might be due to the lower exposure time; hence there is the need in future experiments to expose fibroblast to cancer cells for a longer period of time. This is the first study of this kind on molecular and elemental alteration, which is consistent with increased concentrations in SFs, has been reported for the progression of cancer. In the case of sulfur speciation, despite the observed differences of an increased level of thiols, thioethers and O-linked sulfate, which is consistent with the initial indicator of high cell activity and proliferation, other features appeared unchanged, such as the thiols/disulfide ratio; future experiments will require longer exposure times in co-culture with cancer cells. Future XFI studies should also include other elements such as Fe, Cu, and Zn, as their role in the progression of cancer has been reported, especially that of Zn, which is essential for metalloproteinase activity. These studies help to understand the chemical and phenotype changes in SFs and may contribute to the study of tissue fibrosis, inflammation and cancer progression.

Acknowledgements

We are grateful for a CIHR-Training grant in Health Research Using Synchrotron Techniques (CIHR-THRUST) fellowship and a VINNOVA-VINNMER grant to S.K. The research described in this paper was performed in part at the Canadian Light Source, Saskatoon, Canada, which is supported by the Natural Sciences and Engineering Research Council of Canada, the National Research Council Canada, the Canadian Institutes of Health Research, the Province of Saskatchewan, Western Economic Diversification Canada, and the University of Saskatchewan. This research was also supported by grants from Canadian Light Source. The authors thank Dr. Mark J. Hackett for providing the model sulfur-containing compounds and for critical reading of this paper.

Conflict of Interest

The authors declare no conflict of interest.

Keywords: cancer · fibroblasts · Fourier transform infrared imaging · X-ray absorption spectroscopy · X-ray fluorescence imaging

[1] Z. I. Khamis, Z. J. Sahab, Q.-X. Sang, *Int. J. Breast Cancer* **2012**, *2012*, 574025.

[2] B. Weigelt, J. L. Peterse, L. J. van't Veer, *Nat. Rev. Cancer* **2005**, *5*, 591 – 602.
[3] A. Sadlonova, S. Mukherjee, D. B. Bowe, S. R. Gault, N. A. Dumas, B. A. Van Tine, N. Frolova, G. P. Page, D. R. Welch, L. Novak, A. R. Frost, *Am. J. Pathol.* **2007**, *170*, 1064 – 1076.
[4] R. Kalluri, *Nat. Rev. Cancer* **2003**, *3*, 422 – 433.
[5] M. A. Al-Rakan, D. Colak, S. F. Hendrayani, A. Al-Bakheet, F. H. Al-Mohanna, N. Kaya, O. Al-Malik, A. Aboussekhra, *J. Pathol.* **2013**, *231*, 457 – 465.
[6] R. Kalluri, M. Zeisberg, *Nat. Rev. Cancer* **2006**, *6*, 392 – 401.
[7] S. Kumar, T. S. Shabi, E. Goormaghtigh, *PLoS One* **2014**, *9*, e111137.
[8] E. S. Radisky, D. C. Radisky, *Rev. Endocr. Metab. Disord.* **2007**, *8*, 279 – 287.
[9] A. Aboussekhra, *Int. J. Dev. Biol.* **2011**, *55*, 841 – 849.
[10] A. Chantome, A. Girault, M. Potier, C. Collin, P. Vaudin, J. C. Pages, C. Vandier, V. Joulin, *Exp. Cell Res.* **2009**, *315*, 3620 – 3630.
[11] M. Kedzierska, R. Glowacki, U. Czernek, K. Szydlowska-Pazera, P. Potemski, J. Piekarski, A. Jeziorski, B. Olas, *Mol. Cell. Biochem.* **2013**, *372*, 47 – 55.
[12] N. Traverso, R. Ricciarelli, M. Nitti, B. Marengo, A. L. Furfaro, M. A. Pronzato, U. M. Marinari, C. Domenicotti, *Oxid. Med. Cell. Longevity* **2013**, *2013*, 10.
[13] D. E. Ingber, *Semin. Cancer Biol.* **2008**, *18*, 356 – 364.
[14] D. Liao, Y. Luo, D. Markowitz, R. Xiang, R. A. Reisfeld, *PLoS One* **2009**, *4*, e7965.
[15] S. E. Holton, M. J. Walsh, R. Bhargava, *Analyst* **2011**, *136*, 2953 – 2958.
[16] S. E. Holton, A. Bergamaschi, B. S. Katzenellenbogen, R. Bhargava, *PLoS One* **2014**, *9*, e96878.
[17] M. J. Hackett, S. E. Smith, P. G. Paterson, H. Nichol, I. J. Pickering, G. N. George, *ACS Chem. Neurosci.* **2012**, *3*, 178 – 185.
[18] L. Pascolo, A. Gianoncelli, C. Rizzardi, V. Tisato, M. Salome, C. Calligaro, F. Salvi, D. Paterson, P. Zamboni, *Sci. Rep.* **2014**, *4*, 6540.
[19] M. Verdonck, N. Wald, J. Janssis, P. Yan, C. Meyer, A. Legat, D. E. Speiser, C. Desmedt, D. Larsimont, C. Sotiriou, E. Goormaghtigh, *Analyst* **2013**, *138*, 4083 – 4091.
[20] E. Goormaghtigh, R. Gasper, A. Benard, A. Goldsztein, V. Raussens, *Biochim. Biophys. Acta* **2009**, *1794*, 1332 – 1343.
[21] E. Goormaghtigh in *Infrared Spectroscopy in Encyclopedia of Biophysics* (Ed.: G. K. Roberts), Springer, Berlin, Heidelberg, **2013**, pp. 1049 – 1049.
[22] A. Benard, C. Desmedt, M. Smolina, P. Szternfeld, M. Verdonck, G. Rouas, N. Kheddoumi, F. Rothe, D. Larsimont, C. Sotiriou, E. Goormaghtigh, *Analyst* **2014**, *139*, 1044 – 1056.
[23] B. Ravel, M. Newville, *J. Synchrotron. Radiat.* **2005**, *12*, 537 – 541.
[24] G. George, I. Pickering, EXAFSPAK: a suite of computer programs for analysis of X-ray absorption spectra, SSRL, Stanford, **1995**.
[25] C. Li, S. Kumar, C. Montigny, M. le Maire, A. Barth, *Analyst* **2014**, *139*, 4231 – 4240.
[26] D. Naumann, D. Helm, H. Labischinski, *Nature* **1991**, *351*, 81 – 82.
[27] I. I. Patel, D. A. Shearer, S. W. Fogarty, N. J. Fullwood, L. Quaroni, F. L. Martin, J. Weisz, *Cancer Biol. Ther.* **2014**, *15*, 225 – 235.
[28] V. Sosa, T. Moliné, R. Somoza, R. Paciucci, H. Kondoh, M. E. Lleonart, *Ageing Res. Rev.* **2013**, *12*, 376 – 390.
[29] D. J. Lyman, S. G. Fay, *Ecancermedicalscience* **2014**, *8*, 405.
[30] M. Hammadi, V. Chopin, F. Matifat, I. Dhennin-Duthille, M. Chasseraud, H. Sevestre, H. Ouadid-Ahidouch, *J. Cell. Physiol.* **2012**, *227*, 3837 – 3846.
[31] N. Tajima, K. Schonherr, S. Niedling, M. Kaatz, H. Kanno, R. Schonherr, S. H. Heinemann, *J. Physiol.* **2006**, *571*, 349 – 359.
[32] Z. Saidak, C. Boudot, R. Abdoune, L. Petit, M. Brazier, R. Mentaverri, S. Kamel, *Exp Cell Res.* **2009**, *315*, 2072 – 2080.
[33] H. Ouadid-Ahidouch, M. Roudbaraki, P. Delcourt, A. Ahidouch, N. Joury, N. Prevarskaya, *Am. J. Physiol. Cell Physiol.* **2004**, *287*, C125 – C134.
[34] H. Ouadid-Ahidouch, A. Ahidouch, *J. Membr. Biol.* **2008**, *221*, 1 – 6.
[35] W. F. Wonderlin, K. A. Woodfork, J. S. Strobl, *J. Cell. Physiol.* **1995**, *165*, 177 – 185.
[36] B. Gardner, W. P. Graham, G. S. Gordan, H. F. Loken, A. N. Thomas, J. S. Teal, *J. Clin. Endocrinol. Metab.* **1963**, *23*, 1115 – 1124.
[37] A. Boucharaba, B. Guillet, F. Menaa, M. Hneino, A. J. van Wijnen, P. Clezardin, O. Peyruchaud, *Oncol. Res.* **2009**, *18*, 173 – 184.
[38] E. S. Kim, Y. Cha, M. Ham, J. Jung, S. G. Kim, S. Hwang, R. Kleemann, A. Moon, *Oncogene* **2014**, *33*, 3583 – 3593.
[39] A. P. Asimakopoulou, A. D. Theocharis, G. N. Tzanakakis, N. K. Karamanos, *In Vivo* **2008**, *22*, 385 – 389.
[40] S. S. Skandalis, D. Kletsas, D. Kyriakopoulou, M. Stavropoulos, D. A. Theocharis, *Biochim. Biophys. Acta* **2006**, *1760*, 1217 – 1225.
[41] R. F. Cox, A. Hernandez-Santana, S. Ramdass, G. McMahon, J. H. Harmey, M. P. Morgan, *Br. J. Cancer* **2012**, *106*, 525 – 537.
[42] A. S. Haka, K. E. Shafer-Peltier, M. Fitzmaurice, J. Crowe, R. R. Dasari, M. S. Feld, *Cancer Res.* **2002**, *62*, 5375 – 5380.
[43] R. Baker, K. D. Rogers, N. Shepherd, N. Stone, *Br. J. Cancer* **2010**, *103*, 1034 – 1039.
[44] M. P. Morgan, M. M. Cooke, P. A. Christopherson, P. R. Westfall, G. M. McCarthy, *Mol. Carcinog.* **2001**, *32*, 111 – 117.
[45] D. A. Ribeiro, M. E. A. Marques, D. M. F. Salvadori, *Journal of Endodontics* **2004**, *30*, 593 – 596.
[46] W. W. Huber, W. Parzefall, *Curr. Opin. Pharmacol.* **2007**, *7*, 404.
[47] D. H. Dube, C. R. Bertozzi, *Nat. Rev. Drug Discovery* **2005**, *4*, 477 – 88.

Received: September 6, 2016
Revised: December 1, 2016
Published online on January 9, 2017

